Talanta 79 (2009) 1341–1347

Contents lists available at ScienceDirect

Talanta

journal homepage: www.elsevier.com/locate/talanta

Fracture mechanism of metal electrode integrated on a chip and fabrication of a poly(ethylene terephthalate) electrophoresis microchip

Chong Liu[a,b,*], Jing-Min Li[a], Jun-Shan Liu[a], Li-Ding Wang[a,b], Zhen-Xia Hao[c], Heng-Wu Chen[c]

[a] Key Laboratory for Micro/Nano Technology and System of Liaoning Province, Dalian University of Technology, Dalian, China
[b] Key Laboratory for Precision and Non-traditional Machining Technology of Ministry of Education, Dalian University of Technology, Dalian, China
[c] The Institute of Micro-analytical Systems, Department of Chemistry, Zhejiang University, Zijin'gang Campos, Hangzhou 310058, China

ARTICLE INFO

Article history:
Received 7 April 2009
Received in revised form 27 May 2009
Accepted 28 May 2009
Available online 9 June 2009

Keywords:
Electrode fracture
Polymer deformation behavior
Synchronous observation
Finite element simulation

ABSTRACT

Thermal bonding is an important technique to fabricate polymer electrophoresis microchip. However, the metal electrodes deposited on polymer substrate can readily fracture during the thermal bonding. In this paper, poly(ethylene terephthalate) (PET) was exploited to fabricate the electrophoresis microchip with an integrated gold electrode for amperometric detection. The fracture of the gold electrode was studied through FEA (finite element analysis) simulations, the potentially risk positions on the electrode were shown. The calculation results were tested by bonding experiments and were proven to be consistent with the experiments. Besides, an optimal bonding temperature for PET chip was also presented based on FEA simulations and bonding experiments. Considering the low surface properties of PET, oxygen plasma-assisted thermal bonding technique was used to enhance bonding. Upon treated for 150 s, the PET substrates could be thermally bonded at 62 °C without electrode fracture. The fabricated PET chips were demonstrated for detection of standard glucose solution. Satisfactory reproducibility was achieved, and the RSD values of peak height and migration time of the PET CE chips were 0.51% and 2.17%, respectively.

1. Introduction

Capillary electrophoresis (CE) microchip has gained increasingly attention in recent years. The CE microchip has been developed as an attractive technique for the applications in biological and chemical fields, primarily due to their advantages such as high separation efficiency, low reagent consuming and potential portability [1–6]. CE microchips made of polymers have several merits in comparison to quartz, silica and glass-based microchips, such as less expensive and not fragile, a wide range of materials to be selected, a diverse range of fabrication protocols, and various surface chemistries to match the desired application [3,4]. Therefore, various CE chips have been developed with polymer materials [7–10].

It is well known that hot embossing and thermal bonding are important techniques for fabrication of the polymer microfluidic devices [11]. However, there is a disadvantage when thermal bonding is used to fabricate a polymer electrophoresis microchip integrated with metal electrodes: for most of the polymer materials, the bonding must be conducted near their glass transition temperature (T_g), at which the metal film electrode deposited on polymer substrate can readily be fractured. Fig. 1 shows the fracture on a metal film electrode, which occurs as the thermal bonding temperature is near T_g. The microchip with broken electrodes cannot be used for chemical detection. Ueno et al. [12] presented a method to solve this problem. Firstly, they fabricated the electrodes by deposited gold onto polymer substrate. Subsequently, they used a glass wafer to press the electrodes into the polymer substrate. Finally, thermal bonding was used to seal the chip. Though this method protects the electrodes from fracture, this method is time-consuming and complicated. Furthermore, the mechanism of the electrode fracture was not been studied and presented. Luo et al. [13] also developed a method to protect electrodes. They fabricated a rectangle cavity in polymer substrate and deposited the metal electrode into the cavity. It was obvious that this method was also complicated and labor consuming. The mechanism of electrode fracture was also not discussed.

Poly(ethylene terephthalate) (PET) is an attractive polymer used for CE microchip. Its glass transition temperature (T_g) varies with the crystallization degree of the material, from 75 °C for low-degree crystallized to 220 °C for high-degree crystallized. PET is a hydrophobic polymer with low surface energy. To seal PET chip below its glass transition temperature is difficult. Some scholars used PE as adhesive layer to seal PET substrates at a temperature far less than the glass transition temperature of PET [14,15]. However, sealing with the help of PE adhesive layer produced composite chips with PET/PE/PET structure, resulting in inhomogeneous surface

* Corresponding author.
E-mail address: chongl@dlut.edu.cn (C. Liu).

0039-9140/$ – see front matter © 2009 Published by Elsevier B.V.
doi:10.1016/j.talanta.2009.05.048

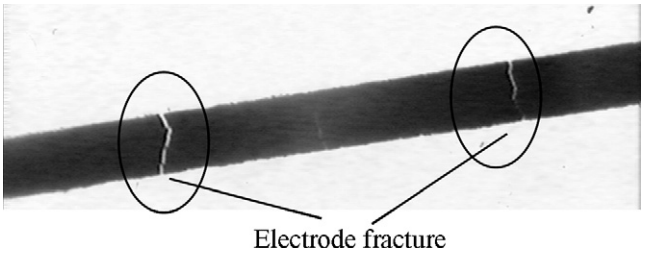

Fig. 1. The photograph of fractured electrode.

properties of the channels. Others used a lamination method to seal PET films [16,17]. This method is time-consuming and costing. Furthermore, it only fits the fabrication of the chips composed of thin films. Thermal bonding is an effective method to fabricate PET chip. However, to protect the integrated electrodes from being fractured, bonding must be conducted at a low temperature, which is difficult.

In this paper, we reported our studies on exploring the PET to fabricate electrophoresis microchip integrated with gold film electrodes, with emphasis being focused on the investigation of electrode fracture and how to avoid it. The causes of the fracture were discussed. The optimal bonding temperature and the locations where fracture would occur were predicted. All the predictions were tested by experiments.

2. Materials and apparatus

2.1. Materials and chemicals

Amorphous PET materials were provided by Dahua Plastic Co. (Hangzhou, China). Its glass transition temperature was 85 °C. Its density was 1.30 g/cm^3. The cover plates, which were prepared from 1 mm PET plate, were cut into 20 mm × 48 mm rectangle pieces with CO_2 laser cutting. The substrates with deposited gold electrodes were all 40 mm × 60 mm × 1 mm rectangle pieces. Microgold film electrodes were fabricated onto the PET substrates with the UV-directed electroless plating technique described in reference [18]. The width of the deposited electrode was 50 μm.

The electrophoresis samples were 99.5% standard glucose solutions (Sigma, St. Louis, MO). NaOH was a 99.99% standard sample (Semiconductor grade, Aldrich). De-ionized water was used throughout the experiments.

2.2. Hot embossing and thermal bonding set-up

A nickel master was fabricated using electroforming technology and used for embossing micropatterns into a PET substrate. The microprotrusions on the mold (microchannels) with "T" feature were 40 μm high and 70 μm wide.

The device used for hot embossing and thermal bonding consisted of a DC torque motor, a screw, two press heads, a linear encoder and a control system. Several TEC (Thermal Electric Cooler) (Ferrotec, Hangzhou Dahe Thermo-Magnetics Co., Ltd.) blocks were placed into the press heads for heating and cooling. The temperature of press heads could be increased to 200 °C. The DC torque motor could provide a control accuracy of 0.5 N and allowed to ensure constant force during the embossing and bonding. A beam load cell was placed under the lower press head to measure the embossing force. A linear encoder was mounted on the movable plate to monitor the displacement of the upper press head. The temperature graph was got by placing two thermocouples into the press heads. All the results were recorded by a computer.

3. Finite element analysis and experimental observation of electrode fracture

3.1. Polymer deformation modes

Finite element analysis was used to simulate the deformation, the stress and the temperature distribution on the electrode during a thermal bonding process.

Because thermal bonding was conducted under polymer glass transition temperature, a visco-plastic model, presented by Argon [19] and modified by Boyce [20], was used to simulate the deformation of glassy polymer. This constitutive model considered the visco-plastic deformation, rate and temperature dependent hardening and softening of glassy polymer. The flow stress in shear was expressed as follows [20].

$$\tau_g = \tilde{S}\left[1 - \frac{kT}{A\tilde{S}}\ln\left(\frac{\dot{\gamma}^p}{\dot{\gamma}_0}\right)\right]^{6/5}, \quad \tilde{S} = S + \alpha_p p \tag{1}$$

where τ was the shear stress, k was the Boltzmann constant, T was the applied absolute temperature, $A\tilde{S}$ was the zero stress level activation energy, $\dot{\gamma}^p$ was the applied shear strain rate, $\dot{\gamma}_0$ was the pre-exponential factor, S was a thermal shear stress, α_p was the pressure coefficient, p was the pressure. An ANSYS software was used to simulate the deformation process. The physical properties and deformations shown in the constitutive model were considered during simulation.

3.2. Finite element analysis model

Fig. 2a shows an illustrative diagram of a polymer electrophoresis microchip integrated with a metal electrode. During a thermal bonding process, the cover plate pressed the electrode severely, especially at the regions of the plate out-side edge and the reservoir in-side edge (shown in Fig. 2). Fig. 2b is a section view achieved by cutting the microchip along the electrode. We established an FEA model, similar with the section view shown in Fig. 2b, to show the deformation and stress. "*L*" was defined as the length of the electrode in the reservoir.

The actual substrate had an initial square shape with dimensions of several tens of millimeters on an edge. To show the microelectrode deformation and stress, three models were established. Fig. 3a shows the first model. We took a rectangle specimen geometry of 50 μm high and 500 μm long as the substrate, a rectangle specimen geometry of 8 μm high and 400 μm long as electrode and

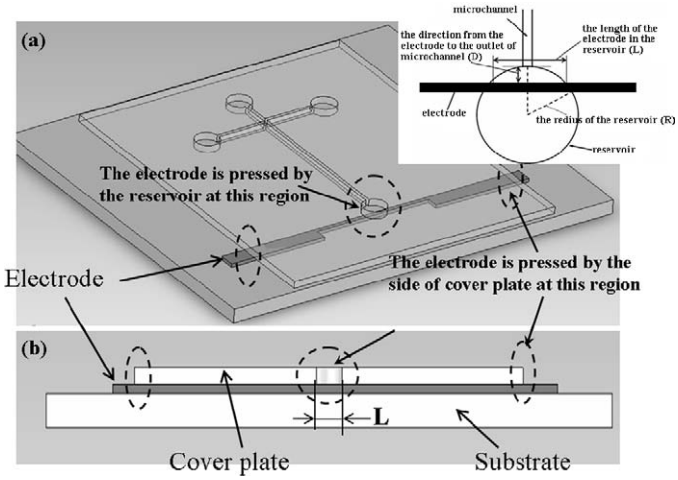

Fig. 2. A schematic of an electrophoresis microchip integrated with a metal electrode. (a) The whole structure of an electrophoresis microchip; (b) the cross-section schematic of the microchip.

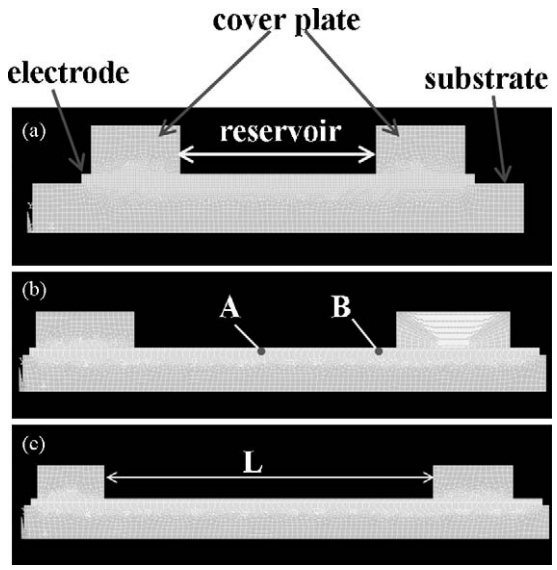

Fig. 3. The meshed model for finite element analysis. (a), (b) and (c) are meshed models as the values of "*L*" are 200 μm, 400 μm and 500 μm.

two-rectangle specimen geometry of 50 μm high and 90 μm long for each as cover plates. The length of the electrode in the reservoir (*L*) was 200 μm. Fig. 3b shows the second model. We took a rectangle specimen geometry of 50 μm high and 800 μm long as the substrate, a rectangle specimen geometry of 8 μm high and 780 μm long as electrode and two-rectangle specimen geometry of 50 μm high and 180 μm long for each as cover plates. The value of *L* was 400 μm. Fig. 3c shows the third model. We used the same parameters of the substrate with the second one except for the cover plates. We took two rectangles specimen geometry of 50 μm high and 165 μm long for each as cover plates. The value of *L* was 500 μm. The space between these two rectangles was used to represent the reservoir. The purpose of establishing three models was to discuss the effects of "*L*" on the electrode fracture. The element was composed of 8 nodes and coupled temperature displacement. To simulate the heating process during thermal bonding, the temperature loads were actived at the bottom line of the substrate and the two top lines of the cover plate. The bottom nodes of the meshed substrate were constrained in the Y-direction. Contact pairs were established between the substrate and electrode. The properties of these contact pairs were set to "bonded" to simulate "deposition of the electrode". Contact pairs also were established between the cover plate and the electrode, and their properties were set to "normal contact". A pressure load (2000 N), which was the same with the pressure used in actual bonding, was applied to the top line of the cover plate.

PET was used as the polymer material for simulation. The mechanical properties of PET were measured by a series of tensile experiments at different temperature. The test shown the elastic modulus of PET at 62 °C, 75 °C and 82 °C were approximate 210.45 MPa, 75.21 MPa and 11.23 MPa, respectively. The yield stresses at 62 °C, 75 °C and 82 °C were 18.32 MPa, 6.24 MPa and 1.82 MPa, respectively. Its coefficient of thermal expansion, thermal conductivity and specific heat were chosen as 7.6e−5 K^{-1}, 0.213 W/(m × K) and 1465 J/(kg × K), respectively. The density of the PET was 1150 kg/m^3, and its coefficient of thermal expansion was 8.9e−5. The material of the electrode was gold. Its density, coefficient of thermal expansion, specific heat and thermal conductivity were 19320 kg/m^3, 14.2e−6, 129 J/(kg × K) and 318 W/(m × K), respectively. Its elastic modulus, yield strength, fracture stress and Poisson ratio were 171 GPa, 205 MPa, 230 MPa and 0.42, respectively.

The temperature dependent shear modulus of glassy PET was given as follows [21].

$$\log \mu = \log(1205.0) - 0.00118(T - 298) \quad (2)$$

where μ was the shear modulus, and T was the applied absolute temperature. The Poisson ratio (ν) for glassy PET was 0.34.

3.3. Procedure for simulation

We conducted three simulations under different bonding conditions:

1. The first simulation was performed under 363 K (82 °C) and 2000 N by using those three models established in Section 3.2. Two points on the electrode (the points "A" and "B" shown in Fig. 3) were selected, and the stress variation on these points was discussed to demonstrate the effects of "*L*" on the electrode fracture.
2. The second simulation was conducted by setting the bonding temperature and pressure to 335 K (62 °C) and 2000 N, respectively. The results got at 62 °C were compared with those got at 82 °C, to show the effects of bonding temperature on electrode fracture.
3. Finally, with the bonding temperature and pressure being respectively changed to 348 K (75 °C) and 2000 N, the last simulation was carried out to achieve the optimal temperature region for PET complete bonding and electrode protection.

3.4. Experimental observation of electrode fracture

First, we studied the effects of temperature on electrode fracture. The steps were as follows:

1. The PET chip integrated with gold electrode was bonded at 82 °C and 2000 N conditions. After releasing from the bonding machine, the electrode topography on the bonded chip was observed with a microscope.
2. The bonding experiments were repeated at 62 °C and 2000 N conditions, and the change of the electrode was observed as described in 1.
3. The results observed at 62 °C were compared with the results obtained at 82 °C to analyze the electrode fracture. The experimental results were also compared with the simulation results to study the mechanism of electrode fracture.
4. We performed bonding experiments at 75 °C and observed the integrated electrode. The optimal bonding temperature was discussed in Section 4.1.

Second, we studied the effect of "*L*" on the electrode fracture. The steps were as follows:

1. The chips were bonded at 82 °C and 2000 N with the varied "*L*" values of 200 μm, 400 μm and 500 μm, respectively.
2. The fracture site on the electrode was recorded, and it was compared with the simulation results to show the effects of "*L*".

4. Results and discussions

4.1. The effects of bonding temperature on electrode fracture

Fig. 4a exhibits the simulation results of bonding PET chip at 82 °C and 2000 N by setting "*L*" to 400 μm. It is observed that the electrode has been pressed to be serpentine at 82 °C and the tensile stress near the reservoir wall is large (Fig. 4a). The value of the tensile stress at the left side of the reservoir wall is approximate

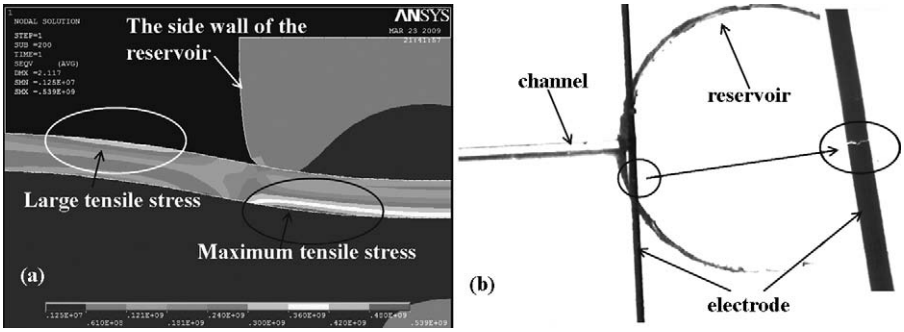

Fig. 4. The results of bonding PET chip at 82 °C. (a) The simulation results of local stress on the electrode at the region near the wall of reservoir; (b) the electrode fracture achieved by bonding at 82 °C and 2000 N.

300–420 MPa. The value of the maximum tensile stress outlined by black circle line is 480–539 MPa. All these stresses have gone beyond the gold fracture stress which is 230 MPa and may result in electrode fracture. Hence, the region near the reservoir wall becomes a potential risk position to occur fracture. Furthermore, the tensile stress near the cover plate side wall is 240–539 MPa, which is also larger than the fracture stress of the gold. Fig. 4b shows the actual photograph of the electrode integrated on PET substrate which is achieved by bonding at 82 °C and adjusting *L* to be approximate 400 μm. The fracture occurs in the region outlined by circle line which is according to the dangerous region predicted by simulation. However, though the electrode deformation is large near the side of the cover plate, no fracture was observed in this region.

When bonding was conduct at 82 °C, the bonding temperature was close to the glass transition temperature of PET. The modulus of PET decreased sharply, which results in large deformation of substrate and cover plate during bonding. Based on the analysis mentioned above, large deformation had more danger to induce electrode fracture. As the bonding temperature was far lower than the glass transition temperature, the modulus kept at a high-level, which resulted in small deformation. We simulated the bonding at 62 °C to show the electrode deformation and stress. Fig. 5 shows the calculation results of bonding at 62 °C and set the value of "*L*" to 400 μm. Fig. 5a shows the whole stress distribution and deformation of the electrode. Fig. 5b shows the local stress and deformation near the reservoir wall. Compared with the results shown in Fig. 4, the stress near the reservoir wall is only 1.17–1.81 MPa, and the maximum tensile is only about 2.11 MPa, which are all far less than the fracture stress of gold. The results indicate that reducing bonding temperature is an effective method to protect electrode from fracturing. Fig. 5c and d shows the electrodes achieved by bonding PET chip at 62 °C. The electrode fracture is not seen. The experimental observation accords with the simulation results. We also simulate the electrode deformation at 75 °C. This simulation is conducted by setting the modulus of the PET as 75.21 MPa. The calculation results show the maximum tensile stress is about 140–160 MPa. Because the maximum tensile stress is only slightly smaller than the fracture stress of gold, bonding at this temperature may also result in electrode fracture. In actual bonding experiments, we observed electrode fracture at this temperature. However, we thought that bonding at this temperature was not good. Based on these discus-

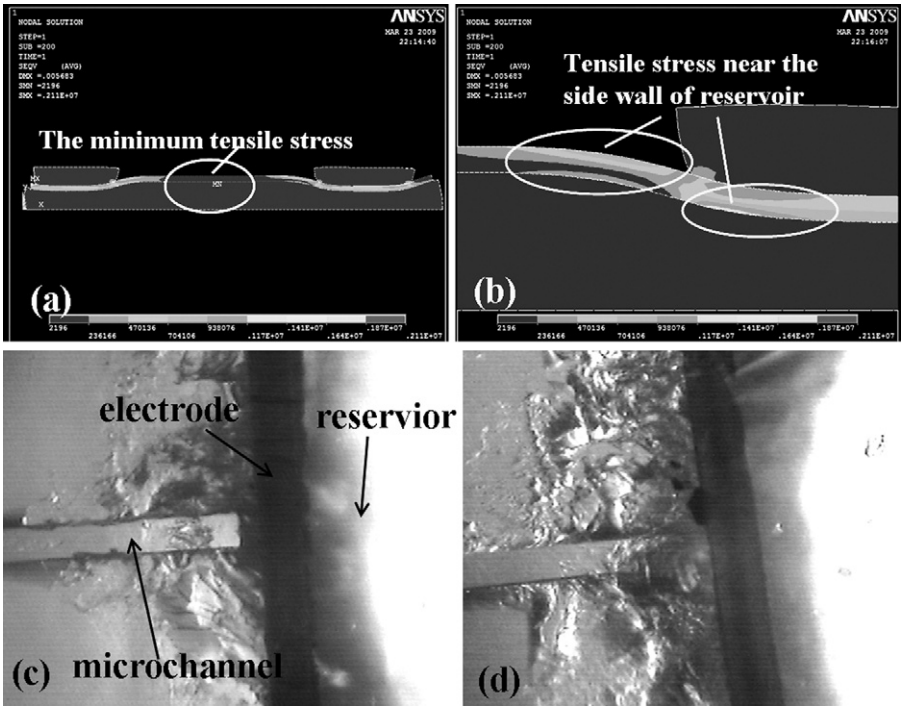

Fig. 5. The results of bonding at 62 °C. (a) The calculation results of whole stress distribution and deformation of the electrode; (b) the calculation results of local stress and deformation on the electrode near the wall of reservoir; (c) and (d) are the electrode achieved by bonding PET chip at 62 °C.

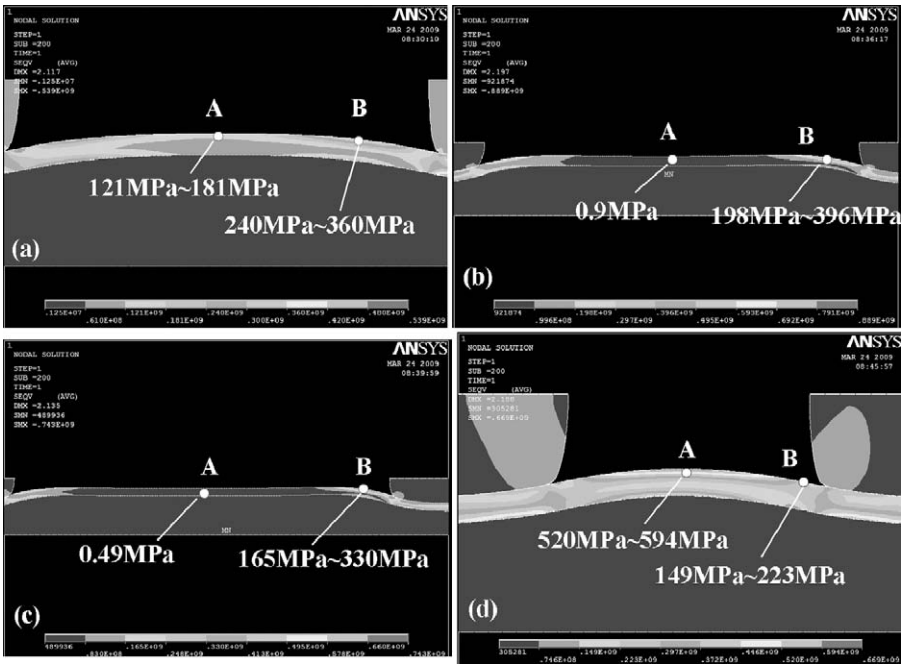

Fig. 6. The simulation results to exhibits the effects of "*L*" on electrode fracture. (a) The stress distribution on electrode as the value of *L* is 200 μm; (b) the stress as *L* is 400 μm; (c) the stress as *L* is 500 μm; (d) the stress as *L* is 100 μm.

sions, we thought the bonding temperature must be lower than 75 °C, and 60–70 °C was ideal.

4.2. The effects of "L" on electrode fracture

"*L*" represents the length of the electrode in the reservoir (shown in Fig. 2). The simulation results indicate the value of "*L*" has significant effects on the stress distribution and deformation of the electrode.

We have chosen two points on the electrode to exhibits the stress variation, point "A" is in the middle of the electrode, point "B" is near the wall of the reservoir, these two points have been shown in Fig. 3b. The tensile stress in point "A" reduces from 121–181 MPa (Fig. 6a) to 0.49 MPa (Fig. 6b) as the value of "*L*" increases from 200 μm to 500 μm. The tensile stress in point "B" remains at 200–300 MPa (Fig. 6a–c) as the value of "*L*" varies from 200 μm to 500 μm. To show the tensile stress variation clearly, we perform another simulation by setting "*L*" to 100 μm. It is found the tensile stress in point "A" is 520–594 MPa, which is far larger than the stress in point "B" (Fig. 6d). From the analysis, we got the following conclusions:

1. The tensile stress in the middle of the electrode reduced as the value of "*L*" increased.
2. The tensile stress near the wall of reservoir remained steady as the value of "*L*" increased. The tensile stress at this region always remained at 200 MPa ~300 MPa, which made it become a risk position to occur fracture.
3. The tensile stress concentration point on the electrode moved from the middle (point A) to the side (point B) as the value of "*L*" increased.

The results as *L* is 400–500 μm has been shown in Fig. 4b. The fracture position is near the predicted position given by simulation. Fig. 7 shows the results achieved by setting "*L*" to 200–300 μm. Some fracture occurs near the reservoir wall, others occur under the reservoir wall. These results also accords with the simulation results. These experiments shown the region near the wall of the reservoir was the most dangerous region to occur electrode fracture. During bonding experiments, we found the fracture occurs in the middle of the electrode, which indicated the tensile stress was smaller than the fracture stress of the gold in this region.

4.3. The deformation mode of the electrode

The deformation behavior of the electrode during thermal bonding has been shown in Fig. 8. Each image corresponds to a different stage of deformation. Fig. 8a shows the state when the bonding starts. The cover plate begins to press the electrode, but the electrode has not deformed. Fig. 8b–d shows the press process. The cover plate presses the electrode from top downwards. Because of the press of cover plate, the polymer materials in substrate are extruded into the space without pressure (the reservoir), which

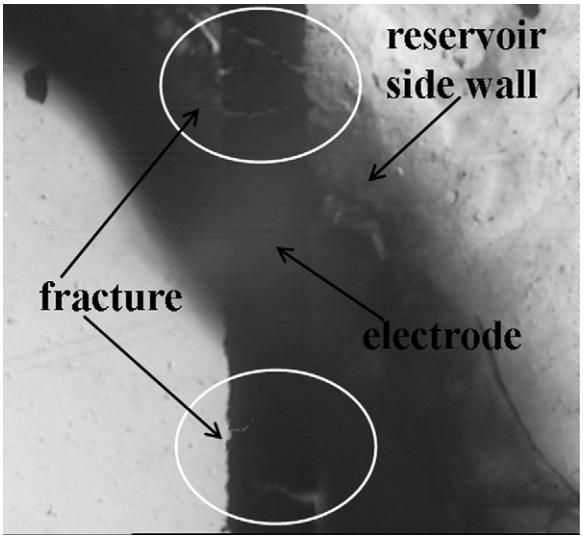

Fig. 7. The bonding experimental results as *L* is 200–300 μm. The electrode fracture has been observed near the wall of the reservoir.

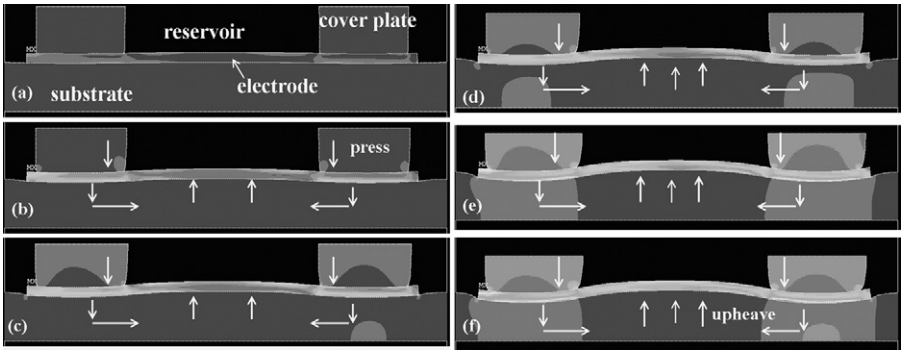

Fig. 8. The calculation results. Each image corresponds to a different stage of deformation. (a) The state when the bonding process starts; (b), (c) and (d) show the press process; (e) the maximum tensile stress has increased above 300 MPa which can result in electrode fracture; (f) the maximum tensile stress reaches its peak, which is about 719 MPa.

results in the electrode is jacked up to form a protrusion (which likes a "hill"). The tensile stress near the wall of reservoir increases above 300 MPa in Fig. 8e, which can result in electrode fracture. In Fig. 8f, the maximum tensile stress reaches its peak, which is about 480–539 MPa.

Because the coefficients of thermal expansion are different between PET and gold, the heating may cause thermal stress between PET substrate and gold electrode. We calculated the value of thermal stress to show its effects. Fig. 9 shows the thermal stress during bonding. We did not add pressure to the electrode and the substrate in this simulation as we only wanted to study the effects induced by thermal stress. Fig. 9a is the whole deformation of the substrate with an integrated gold electrode. Fig. 9b and c are local results to show the stress in the middle of the electrode and at one end of the electrode, respectively. In the middle of the electrode, the tensile stress is only about 1.17–2.40 MPa (Fig. 9b), which is far more less than the fracture stress of the gold. The maximum tensile stress occurs at one end of the electrode, which is shown in Fig. 9c. The value of the maximum tensile stress is about 4.2 MPa. The stress cannot destroy the electrode. However, this tensile stress may separate the electrode from the polymer substrate. Hence, it could be concluded the flow and deformation of the polymer materials during bonding were the main causes of electrode fracture.

4.4. Fabrication of PET electrophoresis microchip without electrode fracture

We used CO_2 laser to fabricate reservoirs on PET cover plate (the plate without electrode). The diameters of the reservoirs were all 2 mm. Subsequently, we used hot embossing to replicate microchannels on the cover plate. The channel had "T" feature. The mold used for replication was produced by UV-LIGA and electroforming. In the previous report [18], the hot embossing of PET chips was performed at the temperature of 70 °C and pressure of 0.5 MPa. In the present work, it was found that the replication precision of microchannel was improved with the increase in embossing temperature. As the temperature increased to 90–100 °C, the replication precision of the channel was good. Unfortunately, the reservoir cells fabricated on the cover plate severely deformed as the embossing temperature increased to above 98 °C. Therefore, the hot embossing should be conducted at about 90 °C so as to get acceptable replicate precision and reduced the risk of the deformation of the reservoir cells.

From the analysis in Section 3.1, we knew that bonding must be conducted at approximate 60–70 °C. It could be found that more than half area of the chip was not sealed. We measured the contact angle of the PET and calculated its surface energy. The surface energy of the untreated PET substrate was only 41.4 nJ/cm^2. To seal the chip entirely was difficult in this surface energy level. Here, we used oxygen plasma surface activation to improve the surface wettability and the surface energy of the PET substrate. The treatment parameters were as follows: the excitation frequency was 13.2 MHz; the RF (radio frequency) power was 60 W; the treatment pressure was 150 Pa; the flow rate of the oxygen gas was 3.5e−7 m^3/s; the treatment time was 150 s. The surface energy of PET increased to 81.2 nJ/cm^2 after the first 100 s treatments, and the contact angle dropped rapidly from 84° to 38°. Minimum contact angle of 34.6° was achieved when the treatment time was 150 s.

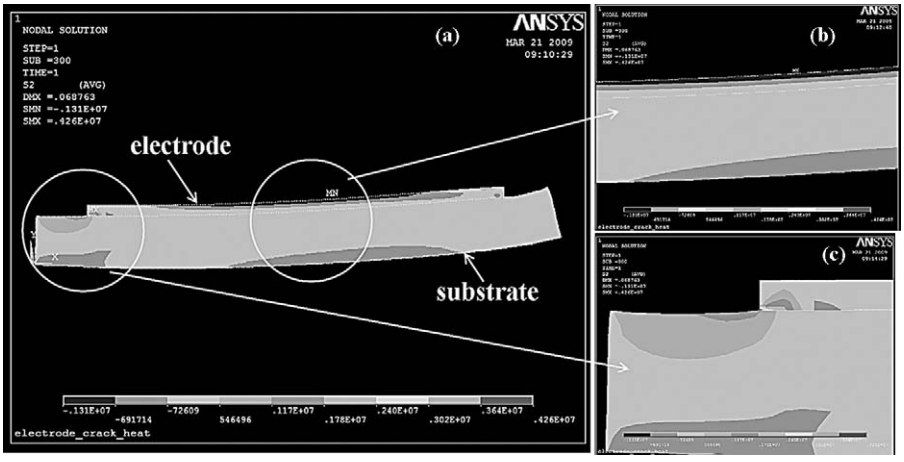

Fig. 9. The thermal stress during bonding. (a) The whole deformation of the substrate with an integrated gold electrode; (b) and (c) are local stress at the regions of middle and one end of the electrode, respectively.

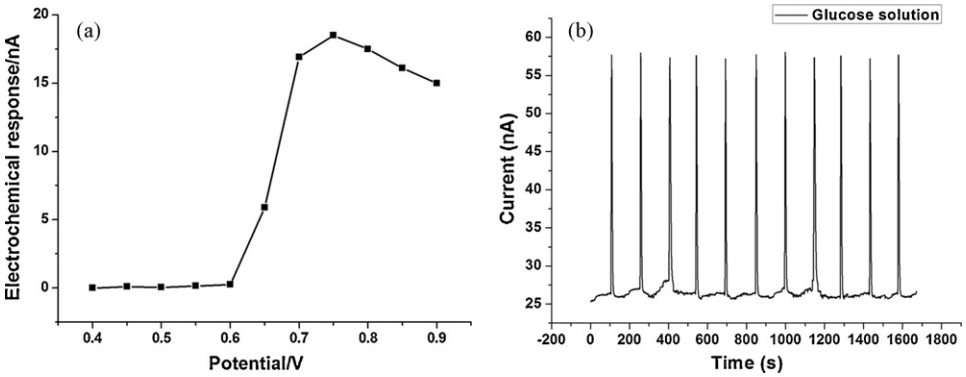

Fig. 10. The application of the chip. (a) Hydrodynamic voltammogram (HDV) for 0.2 mM glucose standard solution to evaluate the effect of working potential on current response; (b) five times consecutive injections of glucose.

However, the contact angle of PET began to increase as the treatment time increased to 180 s. The contact angle increased gradually from 35–38° to 42–45° as the treatment time increased to 200 s. This observation is somewhat different from that of the previous work [18] due to the plasma machine and the experiment conditions adopted in this work are different from those reported in the previous work. Furthermore, several samples of treated PET activated for 150 s were placed in ambient atmosphere for 48 h. The contact angles were found to increase to 50–60°. In contrast, the contact angles for the treated samples which were stored in vacuum conditions changed little (only increased to approximate 40° after being placed under vacuum condition for more than 7 days). This result shown the substrates and chips treated by oxygen plasma must be stored in vacuum.

The treated substrates and cover plate could be sealed entirely. The bonding temperature and pressure were 62 °C and 2000 N, respectively. The fracture strength and shear strength for the bonded PET chip were 130 kPa and 280 kPa, respectively.

4.5. PET chip application

Hydrodynamic voltammogram (HDV) for 0.2 mM glucose standard solution was performed to evaluate the effect of potential applied to the working electrode on current response (Fig. 10a). No significant oxidation currents were observed at the detection potentials lower than 0.55 V. The response current began to increase sharply at the potential of 0.6 V. The HDV exhibited a maximum electrochemical response at 0.75 V. The response current began to decrease as the detection potential was higher than 0.75 V.

Reproducibility was important for the reliability and viability evaluation of microchip. Consecutive injections of glucose were performed to evaluate the reproducibility of PET microchip CE (Fig. 10b). The RSD values of peak height and migration time of PET CE chips for 11 consecutive runs were 0.51% and 2.17%, respectively. Compared with the results reported in references [21] and [22], the RSD value of peak height was smaller than the reports, and the RSD value of migration time was slightly larger than the value reported in reference [21], but smaller than the reports in reference [22]. In conclusion, we demonstrated the PET microchips bonded at low temperature could be employed for the electrophoresis of chemical samples, and the stability and reproducibility of the chips were acceptable.

5. Conclusions

The mechanisms of metal electrode fracture were studied by finite element analysis and bonding experiments. Based on the analysis, the causes for the electrode fracture were the flow and deformation of the polymer under high temperature used for chip bonding. The bonding temperature and the length of the electrode in the reservoir played the key roles for the electrode fracture. The most fragile region of the electrode was near the inside wall of the reservoir, at which the tensile stress had exceeded the fracture stress of gold. It had been found bonding PET chip at the temperature region of 60–70 °C preferential.

To bond PET chip, we used oxygen plasma to modify the surface of PET. The surface energy was improved dramatically, which resulted in bonding temperature decreasing. We fabricated the PET electrophoresis chip at 62 °C and 2000 N. The gold electrode integrated on a PET chip kept unbroken. The fabricated PET chip was exploited for glucose electrophoresis. The RSD values of peak height and migration time were 0.51% and 2.17%, respectively.

Acknowledgments

This work is supported by National Basic Research Program of China (2007CB714502), Major Program of National Natural Science Foundation of China (20890024), National Natural Science Foundation of China (50605006), National High Technology Research and Development Program of China (2007AA04Z302), University Excellent Scholar Project of Liaoning Province “Optimal design method of multi-fields coupled microfluidic chip with complicated structure”.

References

[1] Y.-C. Lin, W.-M. Wu, C.-S. Fan, Lab Chip 4 (2004) 60–64.
[2] C.-C. Wu, R.-G. Wu, J.-G. Huang, Anal. Chem. 75 (2003) 947–952.
[3] M. Castano-Alvarez, M.T. Fernandez-Abedul, Electrophoresis 26 (2005) 3160–3168.
[4] S.A. Soper, S.M. Ford, S.Z. Qi, et al., Anal. Chem. 72 (2000) 643A.
[5] Y. Liu, D.A. MacDonald, X.-Y. Yu, Analyst 131 (2006) 1226–1231.
[6] N.E. Hebert, S.A. Brazill, Lab Chip 3 (2003) 241–247.
[7] A.-L. Liu, F.-Y. He, Y.-L. Hu, Talanta 68 (2006) 1303–1308.
[8] G. Xu, J. Wang, Y. Chen, Lab Chip 6 (2006) 145–148.
[9] R.-H. Horng1, P. Han 1, H.-Y. Chen, J. Micromech. Microeng. 15 (2005) 6–10.
[10] Y.-C. Lin, H.-C. Ho, C.-K. Tseng, J. Micromech. Microeng. 11 (2001) 189–194.
[11] Becker, Holger, Sens. Actuators A: Phys. 83 (2000) 130–135.
[12] K. Ueno, F. Kitagawa, H.B. Kim, et al., Chem. Lett. 29 (2000) 858.
[13] Y. Luo, X.D. Wang, J.S. Liu, et al., Chinese patent, NO. CN1641346A (2005).
[14] J.S. Rossier, A. Schwarz, F. Reymond, et al., Electrophoresis 20 (1999) 727.
[15] J.S. Rossier, R. Ferrigno, H.H. Girault, J. Electroanal. Chem. 492 (2000) 15.
[16] F.Y. He, A.L. Liu, J.H. Yuan, et al., Anal. Bioanal. Chem. 382 (2005) 192.
[17] Z.Y. Wu, N. Xanthopoulos, F. Reymond, et al., Electrophoresis 23 (2002) 782.
[18] Z. Hao, H. Chen, X. Zhu, J. Chromatogr. A 1209 (2008) 246–252.
[19] A.S. Argon, Philos. Mag. 28 (1973) 839–865.
[20] M.C. Boyce, Large Inelastic Deformation of Glassy Polymers, Ph.D. thesis, The Massachusetts Institute of Technology, 1986.
[21] Y. Du, J. Yang, W. Zhou, Electrophoresis 25 (2004) 3853–3859.
[22] G.S. Virdia, R.K. Chutani, P.K. Raob, Sens. Actuators B: Chem. 128 (2008) 422–426.